Available online at www.sciencedirect.com
ScienceDirect
Ceramics International 37 (2011) 9–14
CERAMICS INTERNATIONAL
www.elsevier.com/locate/ceramint

Sintering behavior of nano alumina powder shaped by pressure filtration

M. Aminzare [a], Mehdi Mazaheri [b,*], F. Golestani-fard [a], H.R. Rezaie [a], R. Ajeian [c]

[a] Department of Materials and Metallurgical Engineering, Iran University of Science and Technology, Tehran, Iran
[b] Institute of Physics of Complex Matter, Swiss Federal Institute of Technology Lausanne (EPFL), SB-IPMC-LNNME, PH D2 434 (Bâtiment PH), Station 3 (Boîte A), CH-1015 Lausanne, Switzerland
[c] Department of Physics, Iran University of Science and Technology, Tehran, Iran

Received 16 December 2009; received in revised form 27 January 2010; accepted 12 June 2010
Available online 3 August 2010

Abstract

In the present study, the sintering behavior of a commercial nano alumina powder with an initial particle size of 100 nm was investigated. The shrinkage response of the powder formed by pressure filtration (PF) during non-isothermal sintering was measured in a laser assisted dilatometer at three different heating rates of 2, 10 and 25 °C min^{-1} up to 1400 °C. In order to calculate the activation energy of sintering, constant rate of heating (CRH) was employed and the activation energy was found to be 608 ± 20 kJ mol^{-1} for iso-density method. The heating rate was demonstrated to have a vital role on densification behavior and final grain size. The mean grain size of the full dense specimens decreased from 875 to 443 nm when the heating rate increased from 2 to 25 °C min^{-1}.

Keywords: A. Sintering; D. Al_2O_3; Activation energy; Dilatometry

1. Introduction

Sintering, defined a complicated process consists of different transport mechanism for densification of powder and microstructure enhancement. Powder characteristics including composition, agglomeration tendency, and particle size distribution, sintering methods and forming technique all have significant role in sintering behavior of materials [1–4]. Conditions such as time, temperature and atmosphere are crucial in a typical sintering procedure; hence, it has been investigated widely to optimize these parameters. To bring about a predictable situation for sintering behavior, final density and the domination of a special mechanism have been studied for decades. Computer simulations have been taken into consideration to provide predictable models for sintering stages [5,6]. These methods were not successful in as much as they just focused on one stage of sintering out of three stages, which were: (1) neck forms; (2) neck growth and make a continuous network of pores; (3) pore channels destroyed and grain coarsening happened.

Master sintering curve (MSC) is one of the inspiring and useful approaches to predict and control sintering presented by Su and Johnson [7], based on the combined stage sintering model [8]. Description of sintering behavior for a given powder and prediction of microstructure evolution are possible by using the MSC theory [9–11]. In addition, sinter-ability of different powders also can be compared with the MSC [12]. In the MSC theory, two equal functions (Eq. (3)) are introduced: $\Phi(\rho)$, which is function of density (Eq. (1)) and $\Theta(t,T(t))$, which is as a function of temperature and time (Eq. (2)):

$$\Phi(\rho) = \frac{k}{\gamma \Omega D_0} \int_{\rho_0}^{\rho} \frac{(G_{(\rho)})^n}{3\rho \Gamma_{(\rho)}} \tag{1}$$

$$\Theta(t, T(t)) = \int_0^T \frac{1}{T} \exp\left(\frac{-Q}{RT}\right) dt \tag{2}$$

$$\Phi(\rho) = \Theta(t, T(t)) \tag{3}$$

where Q is apparent activation energy for sintering, R gas constant, T absolute temperature, t time, γ specific surface energy, Ω atomic volume, k Boltzmann constant, G mean grain diameter, D_0 pre-exponential term for the diffusion coefficient,

* Corresponding author. Tel.: +41 21 693 3389; fax: +41 21 693 4470.
E-mail addresses: mehdi.mazaheri@epfl.ch, mmazaheri@gmail.com (M. Mazaheri).

0272-8842/$36.00
doi:10.1016/j.ceramint.2010.07.027

and $n = 3$ or 4 for volume or grain boundary diffusion, respectively. Γ represents all geometric scaling parameters for grain or volume diffusion. $\Theta(t,T(t))$ considers only thermal history parameters (temperature, time) and an apparent activation energy (Q). The relationship between density (ρ) and Θ function is defined as the master sintering curve [12,13].

In the present work, sintering behavior of a nano Al_2O_3 powder with particle size of 100–150 nm shaped via pressure filtration method was studied. The apparent activation energy for sintering calculated by the constant rate of heating (CRH) method and compared with the activation energy, determined from mean residual error (MRE) method. In addition, effect of heating rate on densification, densification rate and final grain size was studied.

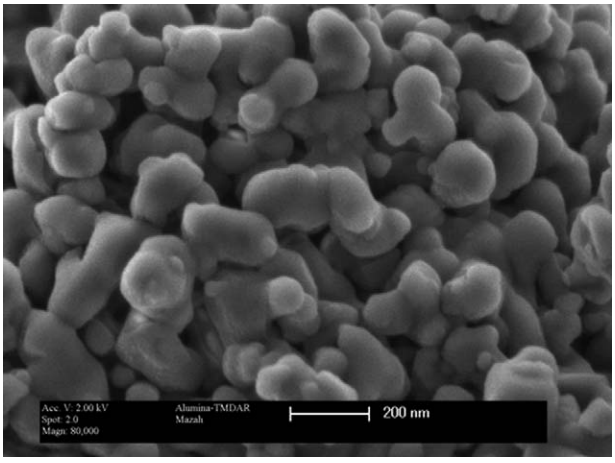

Fig. 1. Scanning electron microscopy of ultra pure alumina powder.

2. Experimental procedures

A pure Al_2O_3 (≥99.99%) powder (Taimei Chemicals Co. Ltd., Tokyo, Japan) was used as raw material. The theoretical density, surface area and primary particle size of powder as reported by supplier was 3.98 g cm^{-3}, 14.5 m^2 g^{-1}, 100 nm, respectively. The powder was stabilized at pH = 10 with a polyelectrolyte (Dolapix CE64, zschimmer-schwarz, lahnstein, Germany) in aqueous slurry with 53 vol% alumina for pressure filtration. The pressure filtration of slurries on an organic membrane with 0.2 μm pore size at a pressure of 40 MPa was preceded in a cylindrical steel die. Detail of pressure filtration method was presented elsewhere [14]. The green density was 63 ± 0.2% theoretical density (TD) using volumetric method. Non-isothermal sintering was performed at different heating rates of 2, 10 and 25 °C min^{-1} by a sinter-dilatometer (TAM 801, NETZCG, Germany).

The microstructure of non-isothermal sintered samples was characterized by scanning electron microscopy (SEM, Philips XL30, Netherlands) after fine polishing using diamond pastes (10, 5, 1 and 0.5 μm) and thermal etching at 1300 °C for 15 min. The grain size of the sintered specimens was determined by multiplying the average linear intercept. For each specimen, 50 line segments were taken into account.

3. Results and discussion

SEM micrograph of the as received powder is shown in Fig. 1. The powders have mainly spherical shape, narrow distribution, and no hard agglomeration can be observed. The initial particle size of the powder is about 100 nm which corresponds to the certificate of factory.

Free strain and densification rate of powder compacts during non-isothermal sintering at three different heating rates of 2, 10 and 25 °C min^{-1} up to 1400 °C are demonstrated in Fig. 2(a) and (b). For calculating the free strain $\varepsilon_{free} = (\varepsilon_z + 2\varepsilon_r)/3$ was applied where ε_z is the longitudinal and ε_r the radial true strains. Fig. 2(a) demonstrates that by increasing the heating rate the temperature at which sintering starts (0.5% shrinkage; T_{onset}) increased. For example, 0.5% shrinkage occurred at 1064 and 1117 °C when heating rate increased from 2 to 25 °C min^{-1}. It proves that the sintering is conducted base on a diffusional base mechanism such as surface diffusion. This kind of behavior is not new and has been previously reported by [15] for nanocrystalline yttria-stabilized zirconia. This tendency is related to the fact that at a lower heating rate, a body is remained for a longer time at each temperature and hence shrinks more than a specimen, which fired by higher heating rate.

Fig. 2(b) shows the evolution of instantaneous densification rate of green bodies for different heating rates as a function of temperature. The maximum densification rates are directly depended on heating rates. It means that, the higher is the heating rate, the higher is the instantaneous densification rate. In addition, the temperature that the maximum densification rate occurred, were changed from 1259 to 1328 °C by increasing the heating rate. It means that, the maximum

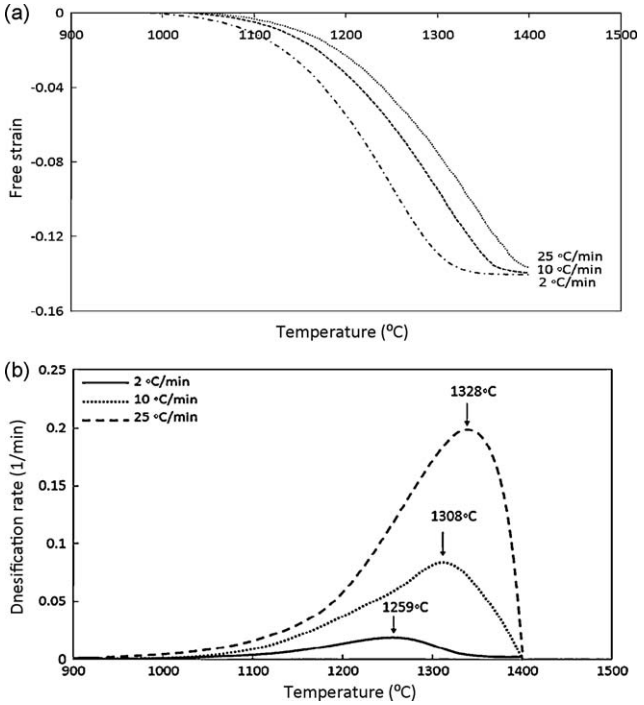

Fig. 2. Effect of heating rate on the free strain (a) and densification rate (b) of alumina compact at three different heating rates.

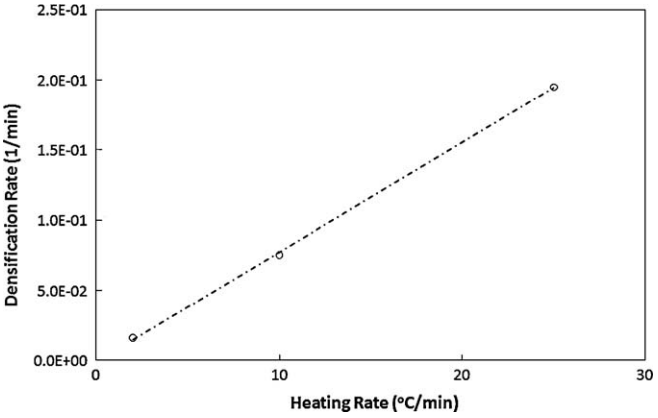

Fig. 3. Maximum densification rate as a function of heating rate.

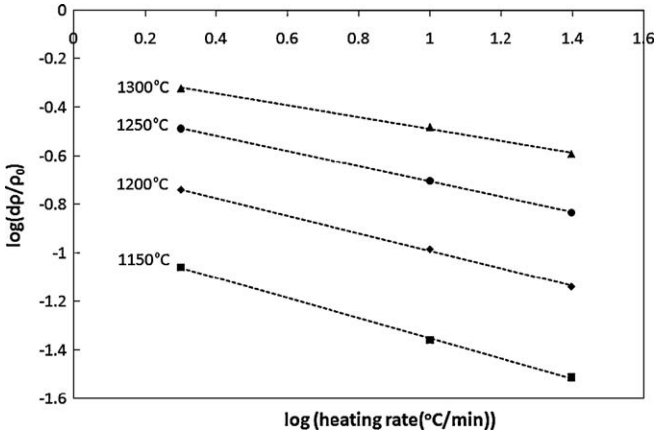

Fig. 5. Density versus heating rate at various temperatures in log scale.

densification was dependent on heating rate of sintering regime. This behavior is also reported by Bernard-Granger and co-worker [16] for alumina samples. But in the case of 3Y-TZP [17] the temperature matches to the maximum quantity of the instantaneous densification rate is almost around 1300 °C and is independent from the heating rate. Linear relationship between the heating rate and the instantaneous densification rate is demonstrated in Fig. 3. This behavior has been reported for 3Y-TZP [17] in the range of heating rate from 100 to 900 °C h^{-1}.

According to Fig. 4, whatever is the heating rate, the strain rate increased to a maximum and then decreased and form a peak. Another point was obtained in this figure, the peak occurs at the range of 83–87% TD which relates to the end of the neck formations step between the crystallites [17]. Hilli et al. [18] has reported similar results for monodoped and mixture doped alumina powders. Additionally, when the heating rate is the lowest the highest final density of the samples is obtained at the end of the sintering process.

Eq. (2) is taking into account for construction of a general curve of sintering so-called Master curve. All parameters are depending on sintering schedule; however, activation energy is unknown. In order to obtain activation energy, constant rate of heating (CRH) method can be useful [19–21]. In CRH method, the densification rate consists of temperature dependent, grain size dependent, and density dependent quantities. In CRH

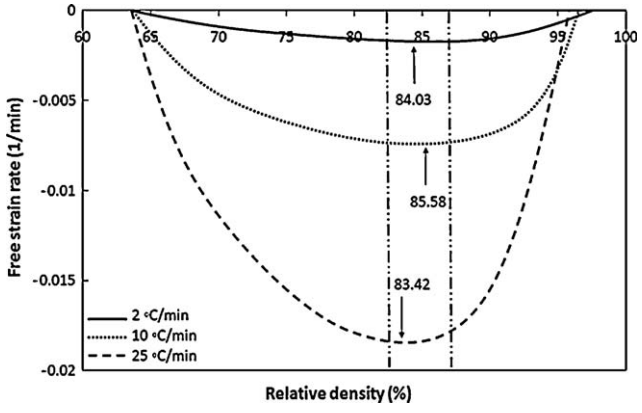

Fig. 4. Free strain rate of the alumina compact as a function of density which different heating rates used.

method there are two different ways to obtain A.E., which are iso-density [22] and iso-strain lines [23,24]. In iso-density lines, the densification rate calculated by Eq. (4):

$$\frac{d\rho}{dt} = A\frac{e^{-Q/RT}}{T}\frac{f(\rho)}{d^n} \tag{4}$$

where $d\rho/dt$ is instantaneous rate of densification, d grain size, n grain size power constant (3 for volume diffusion and 4 for grain boundary diffusion) and $f(\rho)$ only function of density, and A material parameter that is insensitive to d, T, or ρ.

The densification rate can be written as:

$$\frac{d\rho}{dt} = \frac{d\rho}{dT}\frac{dT}{dt} \tag{5}$$

Replacing Eq. (5) in Eq. (4) is resulted to Eq. (6):

$$\ln\left(T\frac{dT}{dt}\frac{d\rho}{dT}\right) = -\frac{Q}{RT} + \ln[f(\rho)] + \ln A - n\ln d \tag{6}$$

The apparent activation energy (Q) can be determined by the slope (by the slope of $-Q/R$) of the straight lines (iso-density) in a plot drawn by the left hand side versus $1/T$ in Eq. (6), if the grain size remains constant. Fig. 5 demonstrates the linear relationship of the density and heating rate (in log–log scale) at intermediate sintering stage (in the range of 70–85% TD). This behavior invokes that the grain growth was inhibited [25,26]. In other words, since we are in intermediate stage of sintering the grain growth is moderately stopped or is very slow. Likewise, microstructural analyses of the alumina powder have shown that the grain growth suppressed in the intermediate stage of sintering [15,27,28].

Fig. 6 illustrates the plots of $\ln[(d\rho/dt) \times T)]$ in function of $1/T$ at different relative densities belong to the rang 70–90%. Apparent activation energy of about 608 ± 20 kJ mol^{-1} obtained from the average slop of the iso-density line in Fig. 6. In other researches the apparent activation energy for sintering of alumina has been reported about 555 and 635 kJ mol^{-1} by Tatami et al. [29] and Sato et al. [30], respectively. In our previous paper, we calculated the activation energy for sintering by using mean residual error methods (MRE) about 700 ± 20 and 605 ± 15 kJ mol^{-1} for

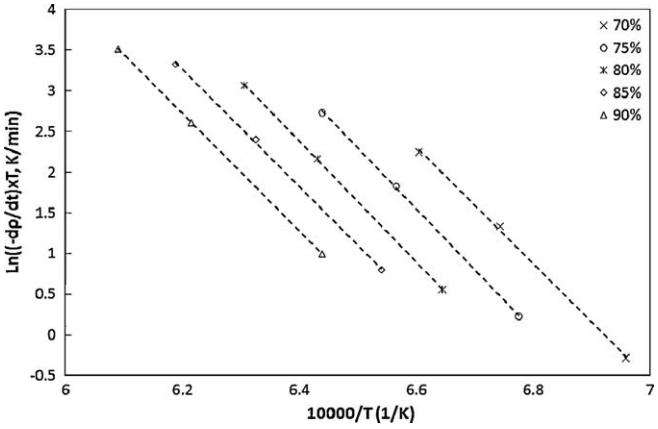

Fig. 6. Plots for the estimate of activation energy via the constant rate of heating method (CRH) iso-density lines from Eq. (6).

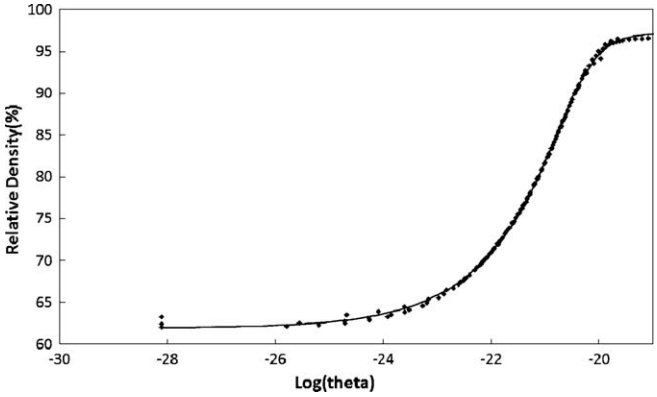

Fig. 7. Master sintering curve for alumina powder prepared by pressure filtration.

cold isostatic (CIP) and pressure filtration (PF) samples, respectively [31].

The activation energy of densification is known as the main characteristic of sintering which can inform the fundamental diffusion mechanism during the sintering process [32,33]. In sum, the values of activation energy announced by other researchers are changed in the range of 440–1100 kJ mol^{-1} [24,29,34,35]. It appears that different processing parameters such as sintering regime, conformation methods and primary powder characteristics affect the sintering mechanism and therefore the activation energy for densification. Shao et al. [36] prepared alumina bodies (initial particle size about 350 nm) by dry pressing at 250 MPa and then sintered at low heating rate of 0.5, 2 and 5 °C min^{-1}. The activation energy about 1064 kJ mol^{-1} was estimated in their study. Wang and Raj [20] obtained activation energy 440 kJ mol^{-1} by heating the samples up to 800 °C in 1 h and with soaking time of 10 min, and then with the heating rate of 5, 10 and 20 °C min^{-1} samples fired to 1600 °C. A value of 1080 kJ mol^{-1} for the activation energy was reported by Fang et al. [35]. They used three heating rates (3, 5 and 10 °C min^{-1}) to reach 1700 °C without any soaking time. Therefore, these indicate that variation in any factors such as initial powder, shaping method and sintering condition may be affect on sintering behavior and activation energy.

Only one diffusion mechanism is considered for construction of MSC [7]. Although, sintering of most materials is combination of different diffusion mechanisms (volume, surface and grain boundary diffusion) [20,36] and the value of activation energy which determined by MSC for sintering mostly can show digression from the known values of the activation energy (activation energy for grain boundary or volume diffusion) and refers to mixture of different mechanisms that govern during sintering [36]. Therefore, other sintering mechanisms can be traced when we found digression at quantity of activation energy. For this purpose, we can apply the MSC to one or several density region and then several activation energies at these regions could be found [31,37]. These values show dominant sintering mechanism at the different density region. Hence, it seems the amounts that we calculated here inform the resultant values for activation energy from beginning to end of the sintering process and so it is contribution of different diffusion process such as surface, grain boundary and volume diffusion. In other words, when one of the diffusion mechanisms is demonstrated in the sintering stages, the other ones were being the limiting steps. Therefore, the present values are not exactly activation energy for grain boundary or volume diffusion or the other ones, but also ''apparent'' activation energy and should be assumed as contribution value between different diffusion mechanisms ''from beginning to end of sintering process''.

Using the above-mentioned activation energy value for sintering (605 ± 15 kJ mol^{-1}), MSC has been constructed (Fig. 7). This indicates that there should have been a general curve, MSC, which used as a practical approach to predict densification under sintering condition.

The MSC curve can be used as a useful tool for designing the best heating profile for getting the desired final density. Table 1 is presented the prediction data's of the sintering time required for alumina samples to attain a certain density at a constant temperature [38] which extracted from MSC curve. For instance, in order to have a 97% relative density, the samples is sintered for 12 min at 1400 °C, or 45 min at 1350 °C, or 3 h at 1300 °C; while it is exceptionable at 1200 °C due to ultra-long time sintering (approximately 3 days).

Fig. 8 illustrates the final microstructure of alumina sample which sintered at 1400 °C with different heating rates. The microstructure observation shows that the heating rate has a distinguished affect on the final grain size of samples. The mean

Table 1
The predictions data for sintering time in seconds for nano alumina green bodies processed via pressure filtration.

Temperature (°C)	Relative density (%)				
	80%	85%	90%	95%	97%
1200	2392	5218	11367	36579	229194
1250	493	1075	2342	7538	47229
1300	112	245	534	1719	10772
1350	28	61	134	430	2694
1400	8	17	36	117	732

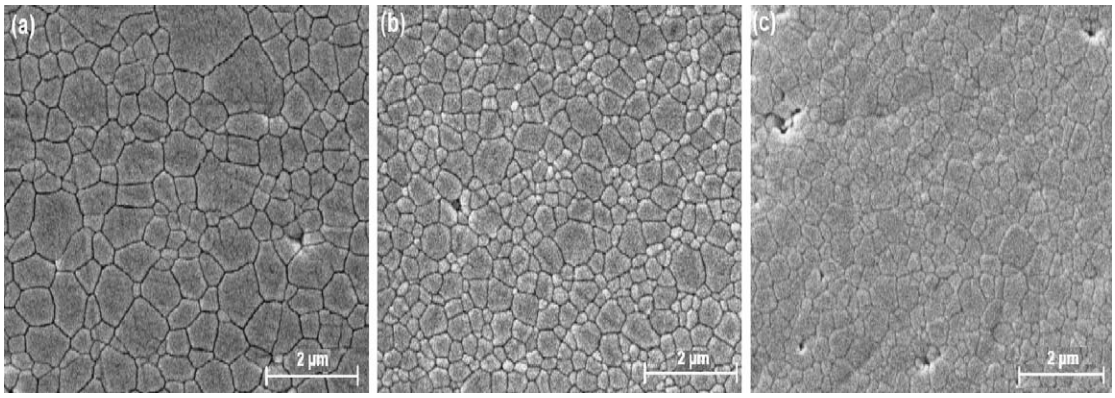

Fig. 8. SEM micrographs of polished and thermally etched surfaces of alumina samples. sintered until 1400 °C with heating rate of 2 (a), 10 (b) and 25 °C min^{-1} (c).

grain size was estimated to be about 875 nm at 2 °C min^{-1}, 650 nm at 10 °C min^{-1} and 443 nm at 25 °C min^{-1}. In addition, samples were composed of polygonal grains, which support the evidence of solid-state sintering.

Based on microstructural observation the effect of heating rate on distribution of the approximately full dense samples at three different heating rates of 2, 10 and 25 °C/min were illustrated in Fig. 9. The reason depicts that the sample which sintered at higher heating rate has most uniformity in microstructure and grain size. The specimens make by lower heating rate have almost wide range of the grain size, however, the specimen that sintered by higher heating rate manifestly exhibits a lower grain size variation. The narrower distribution of the grain size in the samples which heated at 25 °C min^{-1} can be expounded by the higher microstructural homogeneity duo to higher heating rate in comparison with lower heating rate (see Fig. 9). In other words, the heating rate increase can improve the microstructural uniformity of the specimen. Xu et al. [39] have affirmed the precision of this opinion in an experiment about the microwave sintering of ZnO at ultra high heating rates. They reported that with increasing heating rate, the grain size decreased while grain size uniformity increased. Mazaheri et al. [40] have also informed that the heating rate increase amend the microstructural uniformity of the specimen and therefore, increases the fracture toughness of the 8 mol% yttria-stabilized zirconia.

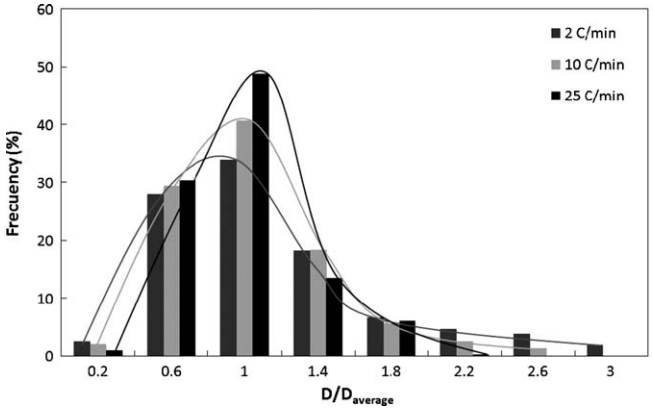

Fig. 9. The grain size distribution of near full dense samples at three different heating rates.

4. Conclusion

In this study non-isothermal sintering of a nano alumina powder was done and the activation energy for densification was estimated. Sintering of alumina was carried out in a sensitive dilatometer at three different heating rates. It was demonstrated that the densification process took place by the conventional solid-state diffusion mechanism in the range of 1050–1400 °C. A MSC curve was constructed for densification data and also the activation energy for sintering by using CRH method was estimated about at 608 ± 20 kJ mol^{-1} for iso-density lines. On the basis of these finding it was concluded that the energy calculated was in fact the so-called apparent activation energy and was estimated to be a contribution of different diffusion mechanisms. The heating rate was found to be effective on grain size and microstructure uniformity.

Acknowledgments

The authors express their gratitude to Dr. O. Guillon for dilatometry measurements and useful advice during the course of this research.

References

[1] Krell, P.k Blan, J. Eur. Ceram. Soc. 16 (1996) 1189–1200.
[2] Legras, C. Carry, P. Bowen, H. Hofmann, J. Eur. Ceram. Soc. 19 (1999) 1967–1978.
[3] M. Azar, P. Palmero, M. Lamnardi, V. Garnier, L. Montanaro, G. Fantazzi, J. Chevalier, J. Eur. Ceram. Soc. 28 (2008) 1121–1128.
[4] A. Krell, J. Klimke, J. Am. Ceram. Soc. 89 (2006) 1985–1992.
[5] R.L. Cobel, J. Appl. Phys. 32 (1961) 787–793.
[6] G.N. Hassold, I.W. Chen, D.J. Srolovit, J. Am. Ceram. Soc. 73 (1990) 2865–2872.
[7] H. Su, D.L. Johnson, J. Am. Ceram. Soc. 79 (1996) 3199–3204.
[8] J. Hansen, R.P. Rusin, M. Teng, D.L. Johnson, J. Am. Ceram. Soc. 75 (1992) 1129–1135.
[9] K.G. Ewsuk, D.T. Ellerby, C.B. Diantanio, J. Am. Ceram. Soc. 89 (2006) 2003–2009.
[10] M.S. Nikalic, V.P. Pavavic, N. Labus, B. Mater, Sci. Forum 494 (2005) 417–422.
[11] C.B. Diantanio, K.G. Ewsuk, Ceram. Trans. 157 (2005) 15–23.
[12] T.R.G. Kutty, K.B. Khan, P.V. Hegde, J. Banerjee, A.K. Sengupta, S. Majumdar, J. Nucl. Mater. 327 (2004) 211–219.

[13] F. Bondioli, A. Bonamartini Corradi, C. Leonelli, T. Manfredini, Mater. Res. Bull. 34 (1999) 2159–2166.
[14] O. Guillon, J. Rodel, J. Am. Ceram. Soc. 90 (2007) 1637–1640.
[15] M. Mazaheri, A. simchi, M. Dourandish, F. Golestani-Fard, Ceram. Int. 35 (2009) 547–554.
[16] G. Bernard-Granger, C. Guizard, J. Mater. Sci. 42 (2007) 6316–6324.
[17] G. Bernard-Granger, C. Guizars, J. Am. Ceram. Soc. 90 (2007) 1246–1250.
[18] N. Hilli, P. Goeuriot, J. Powder Technol. 190 (2009) 129–133.
[19] W.S. Young, I.B. Cutler, J. Am. Ceram. Soc. 53 (1970) 659–663.
[20] J. Wang, R. Raj, J. Am. Ceram. Soc. 73 (1990) 1172–1175.
[21] J. Wang, R. Raj, J. Am. Ceram. Soc. 74 (1991) 1959–1963.
[22] G. Bernard-Granger, C. Guizard, J. Am. Ceram. Soc. 90 (2007) 1246–1250.
[23] F. Raether, J. Am. Ceram. Soc. 92 (2009) 146–152.
[24] F. Raether, P. Schulze Horn, J. Eur. Ceram. Soc. 29 (2009) 2225–2234.
[25] M.-Y. Chu, M.N. Rahaman, L.C.D. Jonghe, R.J. Brook, J. Am. Ceram. Soc. 74 (1991) 1217–1225.
[26] Z.Y. Liu, N.H. Loh, K.A. Khor, S.B. Tor, Scripta Mater. 44 (2001) 1131–1137.
[27] R. Zuo, J. Rodel, Acta Mater. 52 (2004) 3059–3067.
[28] Z. Razavi Hesabi, M. Haghighatzadeh, M. Mazaheri, D. Galusek, S.K. Sadrnezhaad, J. Eur. Ceram. Soc. 29 (2008) 1371–1377.
[29] J. Tatami, Y. Suzuki, T. Wakihara, T. Meguro, K. Komeya, Key Eng. Mater. 317–318 (2006) 11–14.
[30] E. Sato, C. Carry, J. Eur. Ceram. Soc. 15 (1995) 9–16.
[31] M. Aminzare, F. Golestani-fard, O. Guillon, M. Mazaheri, H.R. Rezaie, Mater. Sci. Eng. A 527 (2010) 3807–3812.
[32] M.N. Rahaman, Sintering of Ceramics, CRC Press, USA, 2008.
[33] H.J. Frost, M.F. Ashby, Deformation-mechanism Maps: The Plasticity and Creep of Metals and Ceramics, 2001 (Web version, Chapter 14).
[34] J. Langer, M. Hoffmann, O. Guillon, Acta Mater. 57 (2009) 5454–5465.
[35] T.T. Fang, J.T. Shive, F.S. Shiau, J. Mater. Chem. Phys. 80 (2003) 108–113.
[36] W.Q. Shao, S.O. Chen, D. Li, H.S. Cao, Y.C. Zhang, S.S. Zhang, J. Eur. Ceram. Soc. 29 (2009) 201–204.
[37] Y. Kinemuchi, K. Watari, J. Eur. Ceram. Soc. 28 (2008) 2019–2024.
[38] M.H. Teng, Y.C. Lai, Y.T. Chen, Western Pacific Earth Sci. 2 (2002) 171–180.
[39] G. Xu, I.K. Lloyd, Y. Carmel, T. Olorunyolemi, O.C. Wilson, J. Mater. Res. 16 (2001) 2850–2858.
[40] M. Mazaheri, A.M. Zahedi, M.M. Hejazi, Mater. Sci. Eng. A 492 (2008) 261–267.